Dynein/Sunday driver mediate disorders of dynamic profiles of Golgi outposts induced by amyloid precursor protein

Authors: Qianqian Du[1, 2], Guo Cheng[1, 2], Jin Chang [1, 2], Wei Zhou [1, 2*]

Affiliations

[1] Britton Chance Center for Biomedical Photonics, Wuhan National Laboratory for Optoelectronics-Huazhong University of Science and Technology, Wuhan, Hubei 430074, China

[2] MoE Key Laboratory for Biomedical Photonics, Collaborative Innovation Center for Biomedical Engineering, School of Engineering Sciences, Huazhong University of Science and Technology, Wuhan, Hubei 430074, China

*Correspondence to:

Wei Zhou, wzhou@mail.hust.edu.cn

Tel: + 86 27 87792033-303; + 86 15827641600;

Fax: +86 27 87792034

Abstract

Dendritic abnormality is the pathological hallmark of Alzheimer's disease (AD), but its underlying mechanism remains elusive. Here we showed that amyloid precursor protein (APP), the precursor of β-amyloid, caused dendritic defects in dendritic arborization neurons of *Drosophila* accompanied by Golgi outposts (GOPs) disorders. Half of the dendritic APP co-localized with GOPs, impairing their distribution and compartmental organization; in particular, the dynamic behaviors. By analyzing the state of anterograde/retrograde movements, we found that the motor protein dynein and its adapter protein Sunday driver (Syd) mediated APP-induced dynamic alterations of multi-compartment GOPs (mcGOPs) rather than single-compartment GOPs (scGOPs). Moreover, the loss of *Syd* rescued the defects of dendritic complexity caused by APP. Our findings indicate that APP resident in GOPs disrupts the equilibrium of anterograde/retrograde movements of mcGOPs maintained by dynein/Syd complex, resulting in dendritic abnormalities. This offers new insight into dendritic pathology in AD.

Keywords: APP, dendritic Golgi outposts, Sunday driver, dendritic pathology

Introduction

Alzheimer's disease (AD), characterized by the accumulation of β-amyloid (Aβ) plaque and neurofibrillary tangles in the brain, is one of the most common age-dependent neurodegenerative disorders (Terry, 1996; Terry & Katzman, 1983). Notably, growing evidence shows that dendritic abnormalities, including dystrophic neurites, reduction of dendritic complexity, and loss of dendritic spines, are prominent early-stage phenotypes of AD (SJ Baloyannis, 2009). However, the underlying mechanism remains elusive.

Amyloid precursor protein (APP) is the β-amyloid precursor and plays a significant role in the pathogenesis of AD (J. Hardy & Selkoe, 2002; J. A. Hardy & Higgins, 1992). Mutations of the *APP* gene can induce early-onset familial AD (Golde, Estus, Younkin, Selkoe, & Younkin, 1992), and excess expression of APP is also considered a pathological factor of sporadic AD (Sisodia & Price, 1995). Overexpression of APP results in morphological changes in dendrites, such as reduced dendrite length, bifurcation nodes, and surface area as well as spine density (Alpar et al., 2006; Luebke et al., 2010; Šišková et al., 2014). However, although both APP and related processing enzymes have been found in dendrites (Das et al., 2013; Das et al., 2016; Saraceno et al., 2014), it remains unclear how APP induces the dendritic defects.

Impairments of the structure and function of the Golgi apparatus are implicated in AD. Fragmented Golgi apparatus has been observed in cerebellar Purkinje neurons and hippocampal neurons of AD patients (S Baloyannis, 2002; S. J. Baloyannis, 2014). Meanwhile, the accumulation of Aβ produced by amyloidogenic APP processing has been shown to induce Golgi fragmentation by triggering phosphorylation of Golgi structural proteins such as GRASP65 (Gunjan & Yanzhuang, 2015; Joshi,

55 Chi, Huang, & Wang, 2014).

56 In neurons, the Golgi apparatus is present not only in the soma but also in the dendrites as Golgi
57 outposts (GOPs) (Horton & Ehlers, 2003; Horton et al., 2005; Pierce, Mayer, & Mccarthy, 2001).
58 Functioning as local secretory stations (Horton & Ehlers, 2003; Pierce et al., 2001; Valenzuela & Perez,
59 2015) and acentrosomal microtubule nucleation sites (Ori-McKenney, Jan, & Jan, 2012) in the
60 dendrites, GOPs are required for proper dendrite growth and maintenance. Disruptions to the
61 distribution of GOPs are always accompanied by abnormal dendritic events, such as atypical branching
62 patterns (Ye et al., 2007) and terminal dendrite elongation (Chung et al., 2017). Mutation of Golgi
63 structural protein dGM130, a regulator of the compartmental organization of GOPs, leads to a
64 reduction in high-order dendritic branches (Zhou et al., 2014). Furthermore, time-lapse imaging has
65 revealed that GOPs moving towards dendritic ends and the soma are tightly linked to the extension
66 and retraction of dendritic branches, and disruption of GOPs transport is likely to cause restrained
67 dendrite development and arborization (Arthur, Yang, Abellaneda, & Wildonger, 2015; Lin et al., 2015;
68 Ye et al., 2007). These converging evidence suggests that GOPs contribute to dendritic morphology,
69 an indication that GOPs are involved in APP-induced dendritic defects in AD.

70 To determine how GOPs contribute to dendritic aberrations in the associated pathological events,
71 we investigated the structural and dynamic profiles of GOPs in class III dendritic arborization neurons
72 (C3da neurons) of *Drosophila,* which expressed APP ectopically. First, the colocalization between
73 APP and GOPs was measured and their dynamic profiles were analyzed. Subsequently, dual-color live
74 imaging with *medial*- and *trans*-Golgi markers was used to analyze the compartmental organization
75 and dynamics of GOPs in wild-type and APP-neurons. We further defined the dynamic properties of

76 GOPs affected by APP by manipulating the dynein and kinesin function. Finally, the adaptor protein
77 associated with GOPs dynamic alterations was found by colocalization with GOPs and the rescue of
78 both GOPs dynamic and dendritic shapes.

79 **Results**

80 **APP induces dendritic abnormalities in C3da neurons**

81 To mimic the dendritic pathology in AD, we expressed APP in C3da neurons, a classic model for
82 dendrite development (Grueber, Jan, & Jan, 2002). Firstly, we observed the distribution of APP in
83 neurons by ectopically expressed APP-GFP. With the anti-HRP labeling of the entire neuron shape,
84 APP appeared as punctate patterns and was localized in both dendrites and axon (Figures 1a and b).
85 The quantification of APP-GFP revealed 45.9% ± 4.8% in the dendrites, as well as 54.1% ± 4.8% in
86 the axon (Figure 1c). This implies that nearly half of APP settles as puncta in the dendrites.

87 We then examined how APP influenced the dendritic morphology of C3da ddaA neurons. This
88 showed significant differences in dendritic features between APP-expressing neurons (APP neurons)
89 and wild-type neurons (WT), including the total dendrite length, dendritic branching patterns, as well
90 as the density and length of dendritic spikes (a dendritic spine-like structure in sensory neuron,
91 (Grueber et al., 2002)) (Figure 1d). Specifically, the total dendrite length (Figure 1e; WT: 1,914.7 ±
92 79.7 μm; APP: 1,626.9 ± 54.0 μm) and the number of dendritic branch points (Figure 1f; WT: 14.6 ±
93 1.0; APP: 10.4 ± 0.3) in APP neurons were reduced, which suggest that APP suppresses growth in
94 dendrites. In comparison, most of the reduction for dendritic branch points occurred in high-order
95 branch points (the fourth-order and up; Figure 1g; WT: 4.0 ± 0.5; APP: 2.4 ± 0.4). This means that due
96 to the reduced branching complexity APP restrains dendritic arbor maintenance. Despite the significant

97 decrease in the density of dendritic spikes (Figure 1h; WT: 27.7 ± 1.0 per 100 μm; APP: 17.4 ± 0.8 per
98 100 μm), their length remained similar (Figure 1i; WT: 5.4 ± 0.2 μm; APP: 5.5 ± 0.2 μm). Taken
99 together, these morphological defects indicate that dendrite growth and maintenance are seriously
100 disrupted in APP neurons. Such reductions are consistent with the commonly reported dendritic
101 pathology in AD studies (Alpar et al., 2006; Luebke et al., 2010; Šišková et al., 2014). It implies that
102 APP induces severe dendritic defects in C3da neurons.

103 **APP alters the compartmental organization and distribution of GOPs**

104 To find out why APP caused dendritic defects in C3da neurons, we focused on the dendritic Golgi
105 outposts (GOPs), which are important for the growth and branching of dendrites (Ori-McKenney et
106 al., 2012; Ye et al., 2007). We first examined the correlations between APP and GOPs in C3da neurons
107 using fluorescent protein-tagged APP (APP-GFP) and GalT (GalT-TagRFPt, a *trans*-Golgi marker). In
108 both soma and dendrites, APP puncta were colocalized with Golgi units (Figure 2a). Quantification
109 indicated that the overlapped GalT/APP occupied the majority of GalT (Figure 2b; soma: 90.9% ±
110 2.5%; dendrites: 84.6% ± 3.3%) and half of APP (Figure 2c; soma: 67.6% ± 3.2%; dendrites: 49.6% ±
111 3.4%). In addition, we tested APP-GFP with the *medial*-Golgi marker (ManII-TagRFPt). Similar to
112 GalT results, APP was highly colocalized with ManII (Figures 2b and c; In soma, ManII: 87.0% ± 2.8%
113 and APP: 68.2% ± 3.1%; in dendrites, ManII: 83.0% ± 0.9% and APP: 57.7% ± 4.8%). The
114 colocalization between APP and GOPs points to the fact that the dendritic APP resides in GOPs. This
115 implies that APP may influence dendritic patterning by altering GOPs.

116 We characterized the structure and dynamic of GOPs in APP neurons to determine whether APP
117 modulated GOPs. Considering the coexistence of stacked multi-compartment GOPs (mcGOPs) and

118 punctate single-compartment GOPs (scGOPs) in which the *medial*- and *trans*- cisternae are separated
119 from each other (Zhou et al., 2014), the fluorescently tagged *medial*- and *trans*-Golgi markers (ManII-
120 GFP and GalT-TagRFPt) were simultaneously used to distinguish GOPs with different compartmental
121 organization in dendrites (Figure 2d). We observed that the total number of GOPs in APP neurons,
122 including both mcGOPs and scGOPs reduced by almost half compared with the wild-type (Figure 2e;
123 WT: 16.2 ± 0.8 per 100 μm; APP: 8.0 ± 0.7 per 100 μm). Moreover, the proportions of mcGOPs and
124 scGOPs were inversely associated, with the former increasing (Figure 2f; WT: 32.0% ± 4.0%; APP:
125 48.4% ± 2.9%), while the latter decreased (Figure 2f; WT: 68.0% ± 4.0%; APP: 51.6% ± 2.9%). That
126 implies that APP induces alteration of the compartmental organization of GOPs.

127 We further examined the distribution of GOPs in dendrites. To describe the distribution, the
128 dendrites were divided into three segments depending on the distance to soma: proximal (0 -100 μm),
129 medial (100 - 200 μm), and distal (> 200 μm). Overall, the distribution tendency of mcGOPs showed
130 a pronounced shift between wild-type and APP neurons (Figures 2g and h). Specifically, the mcGOPs
131 were more enriched in the proximal part of dendrite in APP neurons (Figure 2g; proximal: 56.0% ±
132 5.0%; medial:31.7% ± 5.6%; distal:12.3% ± 3.5%), whereas they dominated the distal part in wild-
133 type (Figure 2g; proximal: 23.8% ± 2.7%; medial: 24.4% ± 4.8%; distal:51.8% ± 6.4%). In summary,
134 the compartmental organization and distribution of GOPs are severely disrupted in APP neurons. In
135 particular, the proportion and distribution tendency of mcGOPs change significantly.

136 **APP disrupts the equilibrium of anterograde/retrograde movements of GOPs**

137 GOPs are highly mobile in dendrites (Horton & Ehlers, 2003; Ye et al., 2007), and that could
138 influence the distribution. From the co-expression of APP-GFP and GalT-TagRFPt in C3da neurons,

139 we revealed three different types of puncta in dendrites namely: APP-alone, GOPs-alone, and
140 colocalized APP/GOPs puncta. Using *in vivo* time-lapse imaging, we found that all of them can move
141 bi-directionally (Figure 3a). We also quantified the proportion of mobile GOPs. In APP neurons, the
142 proportion of mobile GOPs decreased from 73.3% ± 4.8% of GOPs-alone puncta to 54.8% ± 5.0% of
143 colocalized APP/GOPs ones (Figure 3b). Besides, the proportion of GOPs-alone puncta was not
144 statistically different between wild-type and APP neurons (Figure 3b), indicating that APP resides in
145 GOPs and alters the movements of GOPs.

146 To clarify how APP affected the dynamic of GOPs, we analyzed the trajectories of GOPs labeled by
147 *medial*- and *trans*-Golgi markers in APP neurons simultaneously (Figures 3c and d), which enabled
148 us to access the compartmental organization of dynamic GOPs. Similar to Figure 3b, the percentage
149 of dynamic GOPs was reduced in APP neurons (Figure 3e; WT: 77.6% ± 2.1%; APP: 64.9% ± 3.1%).
150 We also characterized the behaviors of dynamic GOPs, including direction, displacement, and
151 velocity. GOPs in dendrites have been reported to be able to move bi-directionally: anterograde (from
152 soma to distal dendrite, called as "anterograde GOPs") and retrograde (from distal dendrite to soma,
153 called as "retrograde GOPs"). In wild-type neurons, the proportion of anterograde versus retrograde
154 movements of GOPs was 31.9% ± 1.9% for anterograde to 68.1% ± 1.9% for retrograde, whereas in
155 APP neurons it was 47.1% ± 3.0% to 52.9% ± 3.0% (Figure 3f). This suggests that APP alters the
156 equilibrium of anterograde/retrograde movements of GOPs. We also divided total GOPs into
157 mcGOPs and scGOPs to distinguish the features of dynamic GOPs with different compartmental
158 organizations. It turned out that the change of equilibrium of anterograde/retrograde movements came
159 from both mcGOPs (Figure 3g; WT: anterograde, 38.7% ± 2.4%; retrograde, 61.3% ± 2.4%. APP:

160 anterograde, 49.5% ± 3.1%; retrograde, 50.5% ± 3.1%) and scGOPs (Figure 3h; WT: anterograde,
161 33.8% ± 2.2%; retrograde, 66.2% ± 2.2%. APP: anterograde, 45.5% ± 3.1%; retrograde, 54.5% ±
162 3.1%). We also measured the displacements and velocity of GOPs movements in APP neurons and
163 found only the retrograde displacements were shorter (Figure 3i; WT: mcGOPs / scGOPs, 9.4 ± 1.1 /
164 8.0 ± 0.9 μm; APP: mcGOPs / scGOPs, 5.3 ± 0.6 / 4.7 ± 0.6 μm). Nevertheless, there were no
165 alterations in anterograde displacements and velocity (Figures 3i and j). This showed that more GOPs
166 stayed stationary in APP neurons, whereas the dynamic GOPs tended to have less retrograde
167 movements with shorter displacements.

168 **Dynein mediates the alteration of mcGOPs dynamic induced by APP**

169 The motor proteins are well known to be involved in the positioning of the Golgi complex (Allan,
170 Thompson, & McNiven, 2002; Yadav & Linstedt, 2011). There are two primary motor proteins namely
171 Kinesin and Dynein. Kinesin transports the cargo towards microtubule plus ends, while Dynein
172 mediates the cargo towards minus-ends microtubule (Gibbons, 1981; Hirokawa, 1998; Vale, Reese, &
173 Sheetz, 1985). To find out how motor proteins were involved in dynamic of GOPs, we used RNA-
174 interference to knockdown the motor proteins, including *Dhc (Dhc-64c*, a *dynein heavy chain subunit)*
175 and *Khc* (*kinesin heavy chain*), which have been reported in movements and localization of GOPs in
176 C4da neurons (Kelliher et al., 2018; Lin et al., 2015). The results showed that both *Dhc* RNAi and *Khc*
177 RNAi reduced the proportion of dynamic GOPs (Figures 4a and b; WT: 74.8% ± 2.2%; *Dhc* RNAi:
178 65.5% ± 3.6%; *Khc* RNAi: 53.0 ± 2.8%). Further, we analyzed the direction of movement for dynamic
179 GOPs. To describe the state of anterograde/retrograde movements, we defined the direction index (DI)
180 by calculating the ratio of anterograde to retrograde movements. The results showed that loss of *Dhc*

181 and *Khc* had opposite effects on dynamic GOPs with *Dhc* RNAi decreasing the DI, and *Khc* RNAi
182 increasing it (Figures 4c and d; WT: 0.43 ± 0.03; *Dhc* RNAi: 0.30 ± 0.03; *Khc* RNAi: 0.92 ± 0.13). We
183 also observed that similar to total GOPs, DI for dynamic mcGOPs was downregulated in *Dhc* RNAi
184 and upregulated in *Khc* RNAi (Figure 4e; WT: 0.54 ± 0.07; *Dhc* RNAi: 0.27± 0.03; *Khc* RNAi: 1.20
185 ± 0.24). However, DI for scGOPs dynamic was only regulated by *Khc* RNAi rather than *Dhc* RNAi
186 (Figure 4f; WT: 0.46 ± 0.04; *Dhc* RNAi: 0.52± 0.13; *Khc* RNAi: 1.15 ± 0.25). In addition, under *Dhc*
187 RNAi and *Khc* RNAi, there were no significant changes in the displacements of both mcGOPs (Figure
188 4g; WT: anterograde / retrograde, 6.0 ± 0.8 μm / 7.9 ± 0.8 μm; *Dhc* RNAi: anterograde / retrograde,
189 4.7 ± 0.6 μm / 8.2 ± 0.9 μm; *Khc* RNAi: anterograde / retrograde: 5.3 ± 0.7 μm / 7.8 ± 0.7 μm) and
190 scGOPs (Figure 4h; WT: anterograde / retrograde, 5.4 ± 0.8 μm / 8.7 ± 1.0 μm; *Dhc* RNAi: anterograde
191 / retrograde, 4.5 ± 0.9 μm / 7.2 ± 1.0 μm; *Khc* RNAi: anterograde / retrograde, 5.4 ± 0.9 μm / 8.0 ±
192 1.2μm). This implies that Dynein and Kinesin work together to drive the dynamic of mcGOPs, and
193 maintain the equilibrium between anterograde and retrograde movements.

194 We then examined the dynamic behaviors of GOPs in APP neurons to determine the roles of motor
195 proteins in alterations of GOPs dynamic induced by APP. After the knockdown of Dynein and Kinesin
196 with RNAi, we analyzed the movement directions of GOPs in APP neurons. The results showed that
197 *Dhc* RNAi could rescue the DI of total dynamic GOPs in APP neurons compared with wild-type
198 neurons (Figures 4a and c-d; APP:0.87 ± 0.10; APP+*Dhc* RNAi: 0.52 ± 0.04). Further analyses
199 indicated that *Dhc* RNAi specifically rescued the directional equilibrium of mcGOPs (Figure 4e;
200 APP:1.06 ± 0.07; APP+*Dhc* RNAi: 0.62 ± 0.13) rather than scGOPs (Figure 4f; APP: 0.87 ± 0.09;
201 APP+*Dhc* RNAi: 0.76 ± 0.12). Similarly, *Dhc* RNAi could only rescue the retrograde displacement of

202 dynamic mcGOPs, but not for scGOPs in APP neurons (Figures 4g and h; APP: mcGOPs / scGOPs,
203 5.4 ± 0.6 / 6.0 ± 0.5 μm; APP+*Dhc* RNAi: mcGOPs / scGOPs, 9.1 ± 1.5 /5.8 ± 0.5 μm). Meanwhile,
204 *Khc* RNAi did not affect the alterations of GOPs dynamic induced by APP although it regulated GOPs
205 dynamic (Figures 4a-h). Neither *Dhc* RNAi nor *Khc* RNAi can recover the proportion of dynamic
206 GOPs in APP neurons as shown in Figure 4b. These data suggest that dynein is essential to the pattern
207 of directional movements of mcGOPs induced by APP.

208 Therefore, Kinesin and Dynein jointly regulate the direction of mcGOPs dynamic, of which,
209 dynein mediates the alterations of mcGOPs dynamic induced by APP. The alterations can only be
210 recovered via the loss of dynein.

211 **Sunday driver (Syd) is required for abnormalities of mcGOPs dynamic and dendritic**
212 **arborization induced by APP**

213 The anchoring of motor proteins to the Golgi apparatus is known to be regulated by adaptor
214 proteins (Papoulas, Hays, & Sisson, 2005; Yadav, Puthenveedu, & Linstedt, 2012), which
215 contribute to the various cellular functions. To identify the adaptor protein which was involved in
216 GOPs dynamic in APP neurons, we tested the Sunday driver (Syd), which is located in the post-Golgi
217 vesicles and interacts with both kinesin-I and dynein-dynactin complex (Bowman et al., 2000; Cavalli,
218 Kujala, Klumperman, & Goldstein, 2005).

219 To assess the role of Syd in neurons, we checked the localization of Syd and its function on the
220 density and dynamic of GOPs. First, we generated transgenic flies (UAS::EGFP-Syd) to observe the
221 location of Syd protein in neurons by fusing EGFP with *Syd* cDNA. After the expression of EGFP-Syd
222 in C3da neurons, it was identified in soma and dendrites as puncta and colocalized with Golgi units in

223 soma and dendrites (Figures 5a and b). The density of GOPs was then measured from Syd knockdown
224 (*Syd*-RNAi) and overexpression (OE). Both led to a significant reduction of GOPs density in the
225 dendrites (Figure 5c; density per 100 μm, WT: 9.0 ± 0.6; *Syd* OE: 5.4 ± 0.4; *Syd* RNAi: 7.3 ± 0.4).

226 Further, the properties of GOPs dynamic were examined with *Syd*-RNAi. Results revealed a
227 decline, including proportion of dynamic GOPs (Figures 5d and e; WT: 76.9% ± 2.5%; *Syd* RNAi:
228 55.1% ± 2.7%), and the direction index (DI) of dynamic GOPs (Figures 5f and g; WT: 0.49 ± 0.07;
229 *Syd* RNAi: 0.32 ± 0.02). Notably, those behaviors were dependent on changes of the dynamic of
230 mcGOPs rather than scGOPs (Figures 5h and i; WT: mcGOPs / scGOPs, 0.58 ± 0.11 / 0.53 ± 0.07; *Syd*
231 RNAi: mcGOPs / scGOPs, 0.29 ± 0.03 / 0.67 ± 0.13), which were consistent with those in *Dhc* RNAi
232 (Figures 3d-f). In addition, there were no alterations of the displacements of mcGOPs and scGOPs in
233 *Syd* RNAi (Figures 5j and k; WT: anterograde / retrograde, 4.7 ± 1.3 / 9.1 ± 1.1 μm in mcGOPs and
234 anterograde / retrograde, 6.2 ± 1.2 / 9.5 ± 1.0 μm in scGOPs; *Syd* RNAi: anterograde / retrograde, 5.3
235 ± 0.6 / 7.8 ± 0.6 μm in mcGOPs and anterograde / retrograde, 5.5 ± 1.3 / 7.7 ±1.3 μm in scGOPs).
236 Therefore, Syd plays a critical role in regulating the directional equilibrium of GOPs dynamic,
237 especially for mcGOPs.

238 To determine the contribution of Syd on the alterations of GOPs dynamic induced by APP, we
239 examined the behaviors of dynamic GOPs in APP neurons with knockdown of *Syd*. This showed that
240 the directional equilibrium for dynamic GOPs was recovered in APP neurons where *Syd* was knocked
241 down (Figures 5f and g; APP: 1.06 ± 0.13; APP+ *Syd* RNAi: 0.57 ± 0.04). Besides, this rescue
242 primarily occurred in mcGOPs but not scGOPs (Figures 5h and i; APP: mcGOPs / scGOPs, 1.25 ±
243 0.24 / 1.01 ± 0.13; APP+ *Syd* RNAi: mcGOPs / scGOPs, 0.51 ± 0.07 / 0.76 ± 0.07). However, *Syd*

244 RNAi could not rescue the percentage of dynamic GOPs (Figure 5e; APP: 60.6% ± 2.3%; APP+ *Syd*
245 RNAi: 51.0% ± 3.3%) and the retrograde displacements of GOPs (Figures 5j and k; APP: mcGOPs /
246 scGOPs, 5.2 ± 0.7/ 5.2 ± 0.6 μm; APP+*Syd* RNAi: mcGOPs / scGOPs, 6.1 ± 0.7 / 5.4 ± 0.5 μm). Taken
247 together, Syd is required for the abnormal dynamic behaviors of GOPs induced by APP, especially the
248 equilibrium state of directional mcGOPs dynamic in dendrites.

249 Finally, to clarify the role of Syd on APP-induced dendritic pathology, we observed dendritic
250 morphology in APP neurons with Syd downregulation. Overall, the loss of Syd partially rescued the
251 dendrites phenotype in APP neurons (Figure 6a). In detail, *Syd*-RNAi recovered the number of total
252 branch points (Figure 6c; WT: 12.3 ± 0.3; *Syd* RNAi: 18.5 ± 1.1; APP: 10.3 ± 0.8; APP + *Syd* RNAi:
253 11.4 ± 0.8) and the dendritic complexity (Figure 6d; WT: 3.7 ± 0.3; *Syd* RNAi: 8.5 ± 1.0; APP: 2.1 ±
254 0.4; APP + *Syd* RNAi: 3.6 ± 0.4). However, Syd knockdown did not rescue the total dendrite length in
255 APP neurons (Figure 6b; WT: 1,852.3 ± 48.9 μm; *Syd* RNAi: 2,044.6 ± 80.5 μm; APP: 1,556.6 ± 78.4;
256 APP + *Syd* RNAi: 1,563.8 ± 80.0 μm), and had no recovery on spike density (Figure 6e; density per
257 100 μm: 30.6 ± 0.9 in WT; 17.0 ± 1.0 in *Syd* RNAi; 15.5 ± 2.1 in APP;13.2 ± 0.8 in APP + *Syd* RNAi).
258 Thus, these findings suggest that Syd mediates APP-induced dendritic branching defects by regulating
259 the dynamic behaviors of mcGOPs.

260 **Discussion**

261 In this study, we investigate the cellular mechanism of dendritic pathology in AD by ectopically
262 expressing APP in the C3da neurons of *Drosophila*. The findings suggest that dendritic APP is
263 transported through GOPs and modifies the dynamic profiles of GOPs. GOPs-resident APP breaks the
264 balance of anterograde/retrograde movements of mcGOPs maintained by dynein/Syd complex,

265 resulting in abnormalities of dendritic branching.

266 Here we show that GOPs are involved in APP transportation, and are regulated by APP entry.
267 Previous studies have found that APP secretases such as ADAM10 and BACE-1 exist in GOPs (Das
268 et al., 2013; Das et al., 2016; Saraceno et al., 2014). These suggest that GOPs are involved in the
269 trafficking and processing of APP. Our results show that GOPs co-localize and co-traffick with APP
270 puncta, which confirm that GOPs serve as the carriers of APP trafficking in dendrites. Furthermore, as
271 the local microtubule-organizing centers (Ori-McKenney et al., 2012) and secretory stations (Horton
272 & Ehlers, 2003; Pierce et al., 2001; Valenzuela & Perez, 2015) in the dendrites, GOPs play critical
273 roles in dendrite growth and neurodegenerative diseases (Chung et al., 2017; Lin et al., 2015). Here,
274 we observe that APP induces dendritic defects and severe GOPs deficiencies, including abnormal
275 density, distribution, and dynamic. Collectively, this indicates the involvement of GOPs in neuronal
276 degeneration.

277 The dynamic properties of GOPs are related to neurodegenerative diseases. One of the unique
278 features of GOPs is mobility. A previous study reported that the Parkinson's disease-associated protein
279 Lrrk regulates GOPs dynamic, which is manifested by inhibiting anterograde GOPs movements (Lin
280 et al., 2015). Here, we find that the equilibrium state of the movement direction is a key feature of APP
281 regulated GOPs dynamic. First, we observed that APP residing in GOPs can change their movements,
282 especially the balance of anterograde/retrograde movements. Second, we set up an index DI to quantify
283 the state of GOPs movements, which is equivalent to the ratio of anterograde to retrograde of GOPs
284 movements. We accessed the molecular mechanism of GOPs movements using DI. DI for mcGOPs is
285 downregulated or upregulated when *Dhc* or *Khc* is knocked down. It is worth noting that only the loss

286 of *Dh*c can recover APP-induced DI changes in mcGOPs. Therefore, we conclude that the change of
287 mcGOPs movements caused by APP is dynein-dependent.

288 We consider Syd to be a key molecule in APP regulating mcGOPs dynamic. Previous studies have
289 shown that Syd acts as a bidirectional adaptor interacting with both dynein and kinesin, and regulates
290 the intracellular transport by binding the *kinesin-1* or *dynein-dynactin* complex to cargos (Bowman et
291 al., 2000; Cavalli et al., 2005). In our study, both overexpression and knockdown of Syd decreased the
292 density of GOPs, and loss of it reduced dynamic GOPs and DI of GOPs in dendrites, which implicates
293 the regulation of Syd on the trafficking of GOPs. Moreover, *in vivo* imaging indicated that loss of Syd
294 could rescue DI of mcGOPs in APP neurons, suggesting that Syd is required to the abnormal mcGOPs
295 dynamic induced by APP. Besides, Syd contributes to the suppression of high-order dendrite arbors in
296 APP neurons. Taken together, the dynamic regulation of mcGOPs by Syd is the path for the dendritic
297 defects in APP neurons, providing new insight to understand the dendritic pathology mechanism in
298 AD.

299 Our results also demonstrate the functional differences between mcGOPs and scGOPs. After two
300 types of compartmental organization of GOPs in dendrites were reported (Zhou et al., 2014),
301 Valenzuela and Perez put forward a hypothesis that mcGOPs and scGOPs play different roles in the
302 secretory pathway with mcGOPs responsible for long-distance transport of proteins to dendritic branch
303 points and synaptic junctions, while scGOPs deliver the proteins to the destination, thereby promoting
304 local protein transport to the membrane (Valenzuela & Perez, 2015). Here, we found mcGOPs play
305 important role in neuronal development but scGOPs do not. Our results show that mcGOPs regulate
306 dendritic branching and complexity through the adaptor protein, Syd. Moreover, the results from the

307 loss function of *Dh*c and *Khc* also point that the movement mechanisms between mcGOPs and scGOPs
308 are different. Both *Dhc* and *Khc* can regulate the direction of movement of mcGOPs, while that of
309 scGOPs can only be regulated by *Khc*. Besides, this distinction is also confirmed by the fact that Syd
310 only regulates the movement direction of mcGOPs, but not scGOPs.

311 **Materials and Methods**

312 **Fly Stocks and Transgenic Line**

313 The stocks of flies published in this study included: GAL4$^{19\text{-}12}$ (Xiang et al., 2010); UAS-
314 GalT::TagRFPt and UAS-ManII::TagRFPt/GFP (Ye et al., 2007; Zhou et al., 2014); UAS-CD8::GFP
315 (Lee & Luo, 2001); UAS-APP::GFP^{CG}; UAS-APP695$^{N\text{-}myc}$ and UAS-APP695-Swedish$^{N\text{-}myc}$
316 (Fossgreen et al., 1998); UAS-Dhc64C^{RNAi}, UAS-Khc^{RNAi} and Syd^{RNAi} (Perkins et al., 2015). To
317 generate the UAS-Syd:: EGFP transgenic line, the *Syd* cDNA (#RE24340, BDGP) and *EGFP* cDNA
318 were amplified by PCR and transferred into the vector pJFRC2-10×UAS-IVS-mCD8-GFP (plasmid #:
319 26214, Addgene, Cambridge, MA). The construct was then injected into embryos of PBac{y[+]-attP-
320 3B}VK00033 to generate transgenic flies. All stocks and crosses were maintained in a 25°C incubator
321 with 40-60% humidity.

322 **Dissection, Immunostaining, and Imaging**

323 Third instar larvae were dissected in insect saline and fixed with 4% formaldehyde (PFA) for 40
324 minutes; permeabilized and washed in wash buffer (1X PBS containing 0.15% Triton X-100), and then
325 blocked in 5% normal serum for 30 minutes. After washing, larval fillets were incubated overnight at
326 4°C with the primary antibody and 3 hours with the second antibody at room temperature, avoiding

327 light. The antibodies included: chicken anti-GFP (1:5000, Aves Labs, Inc., Tigard, OR); Alexa647
328 anti-HRP (1:1000; Jackson ImmunoResearch Labs Inc., West Grove, PA); Alexa488 anti-chicken
329 (1:250; Jackson ImmunoResearch Labs Inc., West Grove, PA). The larval fillets were then dehydrated
330 by alcohol and transparentized with xylene before mounting on the slide with DPX (Sigma-Aldrich,
331 St Louis, MO) for imaging. The C3da neurons in the dorsal cluster of the fourth to sixth abdominal
332 segments of the larvae were imaged using a confocal microscope (FV1000, Olympus, Japan) under a
333 60x oil immersion objective (NA=1.42, Olympus, Japan). The images were captured at a resolution of
334 1024*1024 pixels and a z step of 0.4 μm in XYZ mode with sequential scanning. Images of neurons
335 requiring multiple fields were stitched together.

336 **Morphological Analysis**

337 The image analyses were performed by ImageJ (NIH). We measured the fluorescence intensity of
338 APP-GFP to quantify the distribution of APP in the C3da neurons (DeBoer, Dolios, Wang, & Sisodia,
339 2014). The images were corrected for uneven background illumination based on the "rolling ball"
340 algorithm (radius = 50 pixels). To determine the distribution of APP in axon and dendrites, we traced
341 the axon and dendritic arbors separately using line tool with 10-pixels-wide to fit the diameters of axon
342 and dendrites. Then we summed the fluorescence intensity separately in these regions and calculated
343 their proportion. The background intensity was subtracted (calculated in neighbouring area without
344 signal). As the axons of two adjacent C3da neurons (ddaA and ddaF) were closely bundled, we
345 measured both axons and halved the fluorescence intensity value for quantification.

346 For dendritic morphology analyses, we manually traced the dendritic branches by the NeuronJ
347 plugin (Meijering et al., 2004). The tracings were used to measure the length of the dendrite and count

348 the number of dendritic branch points. The number and length of spikes were similarly obtained.

349 To quantify the colocalization between Golgi and APP (or Syd), we calculated the proportion of
350 colocalized puncta. To count the number of total Golgi and total APP (or Syd) as well as the colocalized
351 ones, the Golgi and APP puncta were separately cataloged in ROIs manager, and the puncta that
352 overlapped with the puncta on the other channel were counted as a colocalization (as shown in yellow).
353 For the purposes of analyzing the compartmental organization of GOPs, we classified the colocalized
354 GalT::TagRFPt and ManII::GFP puncta as mcGOPs, while others as scGOPs.

355 ***In Vivo* Imaging**

356 *In vivo* imaging was performed as previously described (Zhou et al., 2014). Firstly, the 3rd instar
357 larvae were collected and anesthetized with ether. The orientation of larvae was adjusted until the
358 ventral trachea was located in the middle of the view field, the larvae were mounted in a drop of
359 halocarbon oil. Larvae were further immobilized by pressing a coverslip mounted on top of vacuum
360 grease. Time-lapse imaging of fluorescently tagged GOPs in C3da neurons was acquired using a
361 confocal microscope (FV1000, Olympus, Japan), 60x oil immersion objective. The settings for the two
362 channels were: ManII (488nm laser for GFP, emission filter: 500-525 nm) and GalT (543 nm laser for
363 RFP, emission filter: BA560IF). Multichannel time-lapse images were captured at zoom 2 with a
364 resolution of 512*512 pixels and collected in XYZT mode for 10 min at 6 s intervals.

365 **Quantification of GOPs Dynamic**

366 To quantify the dynamic behaviors of GOPs, we generated kymograph images (as X-T images
367 shown) using ImageJ. The kymograph images were generated in four steps: stabilization, straightening,

368 reslicing, and timing projection. First, images were stabilized using the Stabilizer plugin (Li, Feb. 2008)
369 to avoid fluctuation from larvae movements. We straightened the dendritic shafts to accurately measure
370 the distances of GOPs movements in the dendrites. The dendrites beyond the first branch points were
371 traced and straightened over the entire stack. The straightened images were resliced to reconstruct the
372 corresponding slices across the time series. Finally, the resliced images were time projected to produce
373 a kymograph of GOPs in the dendrites.

374 Further, we determined the number of dynamic GOPs and analyzed their properties, including
375 direction, displacement, and velocity. We compared the position of GOPs at the start and end of the
376 movement, and classified the movement as anterograde when the final position of GOPs puncta
377 relative to the starting point was towards dendritic ends, and retrograde when the final position of
378 GOPs was towards soma. The coordinates of GOPs trajectories on the kymograph were measured to
379 obtain displacement and velocity information during movements. Meanwhile, the mcGOPs and
380 scGOPs were distinguished based on colocalization analysis for ManII and GalT. Finally, the GOPs
381 trajectories were traced and generated combined tracks of GOPs by aligning the starting points of the
382 tracings, as shown in figures 3d, 4c, 5f. Besides, we defined the difference between dynamic and
383 stationary GOPs and classified them as stationary if they moved less than 0.5 μm in any direction,
384 otherwise as dynamic. To circumvent the influence of the physiological state of neurons and the
385 accuracy of calculation, only kymograph images with at least one moving GOPs were analyzed.

386 **Statistical Analysis**

387 Data were analyzed using a two-tailed Student's *t*-test throughout and p-value was used to
388 determine whether a significant difference existed. Significance levels were presented as follows: *, P
389 < 0.05; **, P < 0.01; ***, P < 0.001; n.s., no significance. Data were presented as mean ± SEM.

390 **Data Availability**

391 The data that support the findings of this study are available from the corresponding author upon
392 reasonable request. The source data underlying Figs. 1c, e-i, 2b-c, e-h, 3b, e-j, 4b, d-h, 5b-c, e, g-k, 6b-
393 f are provided as a source data file.

394 **Acknowledgements**

395 We thank Lei Xue (Tongji University, China), Bing Ye (University of Michigan, Ann Arbor), and
396 Yang Xiang (University of Massachusetts Medical School) for sharing fly stocks and and the Optical
397 Bioimaging Core Facility of WNLO-HUST for support with imaging systems. This work was
398 supported by the National Natural Science Foundation of China (Grant No. 31871027), Science Fund
399 for Creative Research Group of China (Grant No. 61721092), China Postdoctoral Science Foundation
400 founded project (2015T80788), Fundamental Research Funds for the Central Universities/HUST
401 (2017KFXKJC001, 2016YXMS034, 2014TS015), and the Director Fund of WNLO.

402 **Conflict of interests**

403 The authors declare no competing or financial interests.

404 **Authors' contributions**

W.Z. and J.C. conceived this project. W.Z., J.C. and QQ.D. designed the experiments. QQ.D. conducted the experiments and analyzed the data. G.C. carried out molecular experiments. W.Z., J.C. and QQ.D. wrote the paper.

References

Allan, V. J., Thompson, H. M., & McNiven, M. A. (2002). Motoring around the Golgi. *Nature cell biology, 4*(10), E236-E242. doi:10.1038/ncb1002-e236

Alpar, A., Ueberham, U., Bruckner, M. K., Seeger, G., Arendt, T., & Gartner, U. (2006). Different dendrite and dendritic spine alterations in basal and apical arbors in mutant human amyloid precursor protein transgenic mice. *Brain Research, 1099*, 189-198. doi:10.1016/j.brainres.2006.04.109

Arthur, A. L., Yang, S. Z., Abellaneda, A. M., & Wildonger, J. (2015). Dendrite arborization requires the dynein cofactor NudE. *J Cell Sci, 128*(11), 2191-2201. doi:10.1242/jcs.170316

Baloyannis, S. (2002). The Golgi apparatus of Purkinje cells in Alzheimer's disease. *Neuropathology Back to the Roots*, 1-10.

Baloyannis, S. (2009). Dendritic pathology in Alzheimer's disease. *Journal of the Neurological Sciences, 283*(1), 153-157. doi:10.1016/j.jns.2009.02.370

Baloyannis, S. J. (2014). Golgi apparatus and protein trafficking in Alzheimer's disease. *Journal of Alzheimers Disease Jad, 42 Suppl 3*, S153. doi:10.3233/JAD-132660

Bowman, A. B., Kamal, A., Ritchings, B. W., Philp, A. V., McGrail, M., Gindhart, J. G., & Goldstein, L. S. (2000). Kinesin-dependent axonal transport is mediated by the sunday driver (SYD) protein. *Cell, 103*(4), 583-594. doi:10.1016/S0092-8674(00)00162-8

426 Cavalli, V., Kujala, P., Klumperman, J., & Goldstein, L. S. (2005). Sunday Driver links axonal
427 transport to damage signaling. *The Journal of cell biology, 168*(5), 775-787.
428 doi:10.1083/jcb.200410136
429 Chung, C. G., Kwon, M. J., Jeon, K. H., Han, M. H., Park, J. H., Cha, I. J., . . . Kim, G. R. (2017).
430 Golgi outpost synthesis impaired by toxic polyglutamine proteins contributes to dendritic
431 pathology in neurons. *Cell reports, 20*(2), 356-369. doi:10.1016/j.celrep.2017.06.059
432 Das, U., Scott, D. A., Ganguly, A., Koo, E. H., Tang, Y., & Roy, S. (2013). Activity-induced
433 convergence of APP and BACE-1 in acidic microdomains via an endocytosis-dependent
434 pathway. *Neuron, 79*(3), 447-460. doi:10.1016/j.neuron.2013.05.035
435 Das, U., Wang, L., Ganguly, A., Saikia, J. M., Wagner, S. L., Koo, E. H., & Roy, S. (2016).
436 Visualizing APP and BACE-1 approximation in neurons yields insight into the amyloidogenic
437 pathway. *Nature neuroscience, 19*(1), 55. doi:10.1038/nn.4188
438 DeBoer, S. R., Dolios, G., Wang, R., & Sisodia, S. S. (2014). Differential release of beta-amyloid
439 from dendrite- versus axon-targeted APP. *J Neurosci, 34*(37), 12313-12327.
440 doi:10.1523/JNEUROSCI.2255-14.2014
441 Fossgreen, A., Bruckner, B., Czech, C., Masters, C. L., Beyreuther, K., & Paro, R. (1998).
442 Transgenic Drosophila expressing human amyloid precursor protein show gamma-secretase
443 activity and a blistered-wing phenotype. *Proc Natl Acad Sci U S A, 95*(23), 13703-13708.
444 doi:10.1073/pnas.95.23.13703
445 Gibbons, I. R. (1981). Cilia and flagella of eukaryotes. *J Cell Biol, 91*(3 Pt 2), 107s-124s.
446 doi:10.1083/jcb.91.3.107s
447 Golde, T. E., Estus, S., Younkin, L. H., Selkoe, D. J., & Younkin, S. G. (1992). Processing of the

448 amyloid protein precursor to potentially amyloidogenic derivatives. *Science, 255*(5045), 728-
449 730. doi:10.1126/science.1738847
450 Grueber, W. B., Jan, L. Y., & Jan, Y. N. (2002). Tiling of the Drosophila epidermis by multidendritic
451 sensory neurons. *Development, 129*(12), 2867-2878.
452 Gunjan, J., & Yanzhuang, W. (2015). Golgi defects enhance APP amyloidogenic processing in
453 Alzheimer's disease. *Bioessays, 37*(3), 240-247. doi:10.1002/bies.201400116
454 Hardy, J., & Selkoe, D. J. (2002). The Amyloid Hypothesis of Alzheimer's Disease: Progress and
455 Problems on the Road to Therapeutics. *Science, 297*(5580), 353-356.
456 doi:10.1126/science.1072994
457 Hardy, J. A., & Higgins, G. A. (1992). Alzheimer's disease: the amyloid cascade hypothesis. *Science,*
458 *256*(5054), 184-185. doi:10.1126/science.1566067
459 Hirokawa, N. (1998). Kinesin and dynein superfamily proteins and the mechanism of organelle
460 transport. *Science, 279*(5350), 519-526. doi:10.1126/science.279.5350.519
461 Horton, A. C., & Ehlers, M. D. (2003). Dual modes of endoplasmic reticulum-to-Golgi transport in
462 dendrites revealed by live-cell imaging. *Journal of Neuroscience, 23*(15), 6188-6199.
463 doi:10.1523/JNEUROSCI.23-15-06188.2003
464 Horton, A. C., Rácz, B., Monson, E. E., Lin, A. L., Weinberg, R. J., & Ehlers, M. D. (2005).
465 Polarized secretory trafficking directs cargo for asymmetric dendrite growth and
466 morphogenesis. *Neuron, 48*(5), 757-771. doi:10.1016/j.neuron.2005.11.005
467 Joshi, G., Chi, Y., Huang, Z., & Wang, Y. (2014). Aβ-induced Golgi fragmentation in Alzheimer's
468 disease enhances Aβ production. *Proceedings of the National Academy of Sciences of the*
469 *United States of America, 111*(13), 1230-1239. doi:10.1073/pnas.1320192111

470 Kelliher, M. T., Yue, Y., Ng, A., Kamiyama, D., Huang, B., Verhey, K. J., & Wildonger, J. (2018).
471 Autoinhibition of kinesin-1 is essential to the dendrite-specific localization of Golgi outposts.
472 *J Cell Biol, 217*(7), 2531-2547. doi:10.1083/jcb.201708096
473 Lee, T., & Luo, L. (2001). Mosaic analysis with a repressible cell marker (MARCM) for Drosophila
474 neural development. *Trends Neurosci, 24*(5), 251-254. doi:10.1016/s0166-2236(00)01791-4
475 Li, K. (Feb. 2008). The Image Stabilizer Plugin for ImageJ [Online]. Retrieved from
476 http://www.cs.cmu.edu/~kangli/code/Image_Stabilizer.html
477 Lin, C. H., Li, H., Lee, Y. N., Cheng, Y. J., Wu, R. M., & Chien, C. T. (2015). Lrrk regulates the
478 dynamic profile of dendritic Golgi outposts through the golgin Lava lamp. *J Cell Biol,*
479 *210*(3), 471-483. doi:10.1083/jcb.201411033
480 Luebke, J. I., Weaver, C. M., Rocher, A. B., Rodriguez, A., Crimins, J. L., Dickstein, D. L., . . . Hof,
481 P. R. (2010). Dendritic vulnerability in neurodegenerative disease: insights from analyses of
482 cortical pyramidal neurons in transgenic mouse models. *Brain Structure and Function, 214*(2-
483 3), 181-199. doi:10.1007/s00429-010-0244-2
484 Meijering, E., Jacob, M., Sarria, J. C., Steiner, P., Hirling, H., & Unser, M. (2004). Design and
485 validation of a tool for neurite tracing and analysis in fluorescence microscopy images.
486 *Cytometry A, 58*(2), 167-176. doi:10.1002/cyto.a.20022
487 Ori-McKenney, K. M., Jan, L. Y., & Jan, Y.-N. (2012). Golgi outposts shape dendrite morphology by
488 functioning as sites of acentrosomal microtubule nucleation in neurons. *Neuron, 76*(5), 921-
489 930. doi:10.1016/j.neuron.2012.10.008
490 Papoulas, O., Hays, T. S., & Sisson, J. C. (2005). The golgin Lava lamp mediates dynein-based Golgi
491 movements during Drosophila cellularization. *Nat Cell Biol, 7*(6), 612-618.

492 doi:10.1038/ncb1264

493 Perkins, L. A., Holderbaum, L., Tao, R., Hu, Y., Sopko, R., McCall, K., . . . Shim, H.-S. (2015). The
494 transgenic RNAi project at Harvard Medical School: resources and validation. *Genetics,*
495 *201*(3), 843-852. doi:10.1534/genetics.115.180208

496 Pierce, J. P., Mayer, T., & Mccarthy, J. B. (2001). Evidence for a satellite secretory pathway in
497 neuronal dendritic spines. *Current Biology Cb, 11*(5), 351-355. doi:10.1016/S0960-
498 9822(01)00077-X

499 Saraceno, C., Marcello, E., Di Marino, D., Borroni, B., Claeysen, S., Perroy, J., . . . Di Luca, M.
500 (2014). SAP97-mediated ADAM10 trafficking from Golgi outposts depends on PKC
501 phosphorylation. *Cell Death Dis, 5*, e1547. doi:10.1038/cddis.2014.492

502 Šišková, Z., Justus, D., Kaneko, H., Friedrichs, D., Henneberg, N., Beutel, T., . . . von der Kammer,
503 H. (2014). Dendritic structural degeneration is functionally linked to cellular
504 hyperexcitability in a mouse model of Alzheimer's disease. *Neuron, 84*(5), 1023-1033.
505 doi:10.1016/j.neuron.2014.10.024

506 Sisodia, S. S., & Price, D. (1995). Role of the beta-amyloid protein in Alzheimer's disease. *The*
507 *FASEB Journal, 9*(5), 366-370. doi:10.1096/fasebj.9.5.7896005

508 Terry, R. D. (1996). The pathogenesis of Alzheimer disease: an alternative to the amyloid hypothesis.
509 *Journal of Neuropathology & Experimental Neurology, 55*(10), 1023-1025.
510 doi:10.1097/00005072-199655100-00001

511 Terry, R. D., & Katzman, R. K. (1983). Senile dementia of the Alzheimer type. *Annals of Neurology,*
512 *14*(5), 497-506. doi:10.1002/ana.410140502

513 Vale, R. D., Reese, T. S., & Sheetz, M. P. (1985). Identification of a novel force-generating protein,

514 kinesin, involved in microtubule-based motility. *Cell, 42*(1), 39-50. doi:10.1016/s0092-
515 8674(85)80099-4
516 Valenzuela, J. I., & Perez, F. (2015). Diversifying the secretory routes in neurons. *Frontiers in*
517 *Neuroscience, 9*. doi:10.3389/fnins.2015.00358
518 Xiang, Y., Yuan, Q., Vogt, N., Looger, L. L., Jan, L. Y., & Jan, Y. N. (2010). Light-avoidance-
519 mediating photoreceptors tile the Drosophila larval body wall. *Nature, 468*(7326), 921-926.
520 doi:10.1038/nature09576
521 Yadav, S., & Linstedt, A. D. (2011). Golgi positioning. *Cold Spring Harb Perspect Biol, 3*(5).
522 doi:10.1101/cshperspect.a005322
523 Yadav, S., Puthenveedu, M. A., & Linstedt, A. D. (2012). Golgin160 recruits the dynein motor to
524 position the Golgi apparatus. *Dev Cell, 23*(1), 153-165. doi:10.1016/j.devcel.2012.05.023
525 Ye, B., Zhang, Y., Song, W., Younger, S. H., Jan, L. Y., & Jan, Y. N. (2007). Growing dendrites and
526 axons differ in their reliance on the secretory pathway. *Cell, 130*(4), 717-729.
527 doi:10.1016/j.cell.2007.06.032
528 Zhou, W., Chang, J., Wang, X., Savelieff, M. G., Zhao, Y., Ke, S., & Ye, B. (2014). GM130 is
529 required for compartmental organization of dendritic golgi outposts. *Current Biology, 24*(11),
530 1227-1233. doi:10.1016/j.cub.2014.04.008

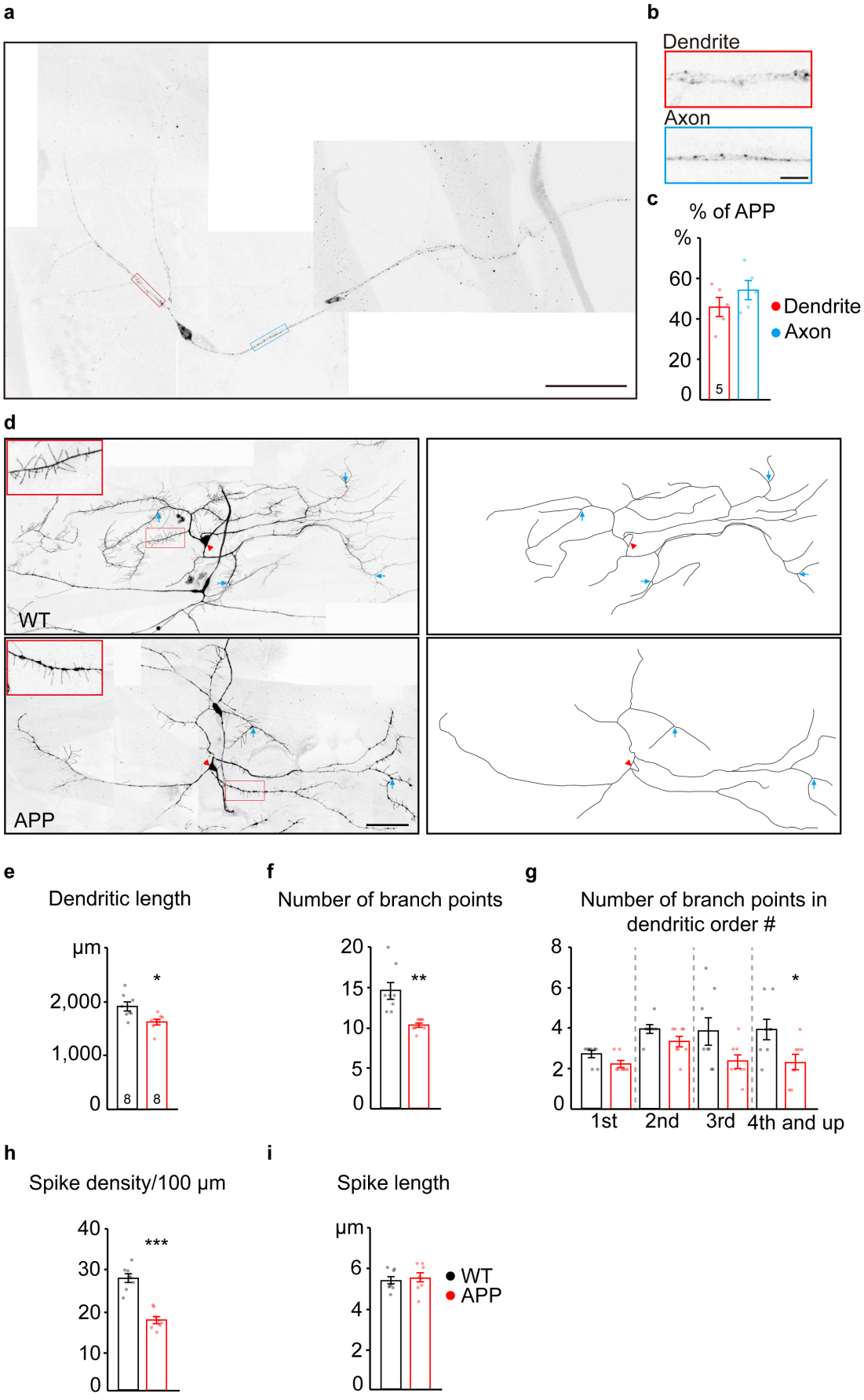
a
b
Dendrite
Axon
c
% of APP
%
60
40
20
0
5
Dendrite
Axon
d
WT
APP
e
Dendritic length
µm
2,000
1,000
0
8
8
*
f
Number of branch points
20
15
10
5
0
**
g
Number of branch points in dendritic order #
8
6
4
2
0
1st
2nd
3rd
4th and up
*
h
Spike density/100 µm
40
30
20
10
0
***
i
Spike length
µm
6
4
2
0
WT
APP

532 **Fig. 1. APP induces dendritic abnormalities in C3 dendritic arborization (da) ddaA neurons.**

533 **(a)** The distribution of APP-GFP in C3da neuron of 3rd instar larva in *Drosophila*. The insets indicate dendrite (red)
534 and axon (blue) respectively. Scale bar: 50 μm. **(b)** Magnified insets in **(a)** exhibit APP-GFP in the dendrite and axon.
535 Scale bar for dendrite and axon: 5 μm. **(c)** The proportion of APP-GFP in the axon and dendrite. (**d)** The morphologies
536 of wild-type (WT) and APP C3da ddaA neurons. Raw images (left) and tracings of dendritic branches (right, the
537 numerous F-actin-based "dendritic spikes" of C3da neurons are not included). The red insets show magnified
538 dendritic spikes. The red arrowhead points to the soma and blue to the branch points of the 4th order and up. Scale
539 bar: 50 μm. **(e-j)** Quantification of dendritic morphologies in wild-type and APP neurons. **(e)** The total dendrite length,
540 **(f)** the number of total branch points, **(g)** the number of branch points in different orders; **(h-i)** The characteristics of
541 dendritic spikes: **(h)** density / 100 μm, **(i)** average length.

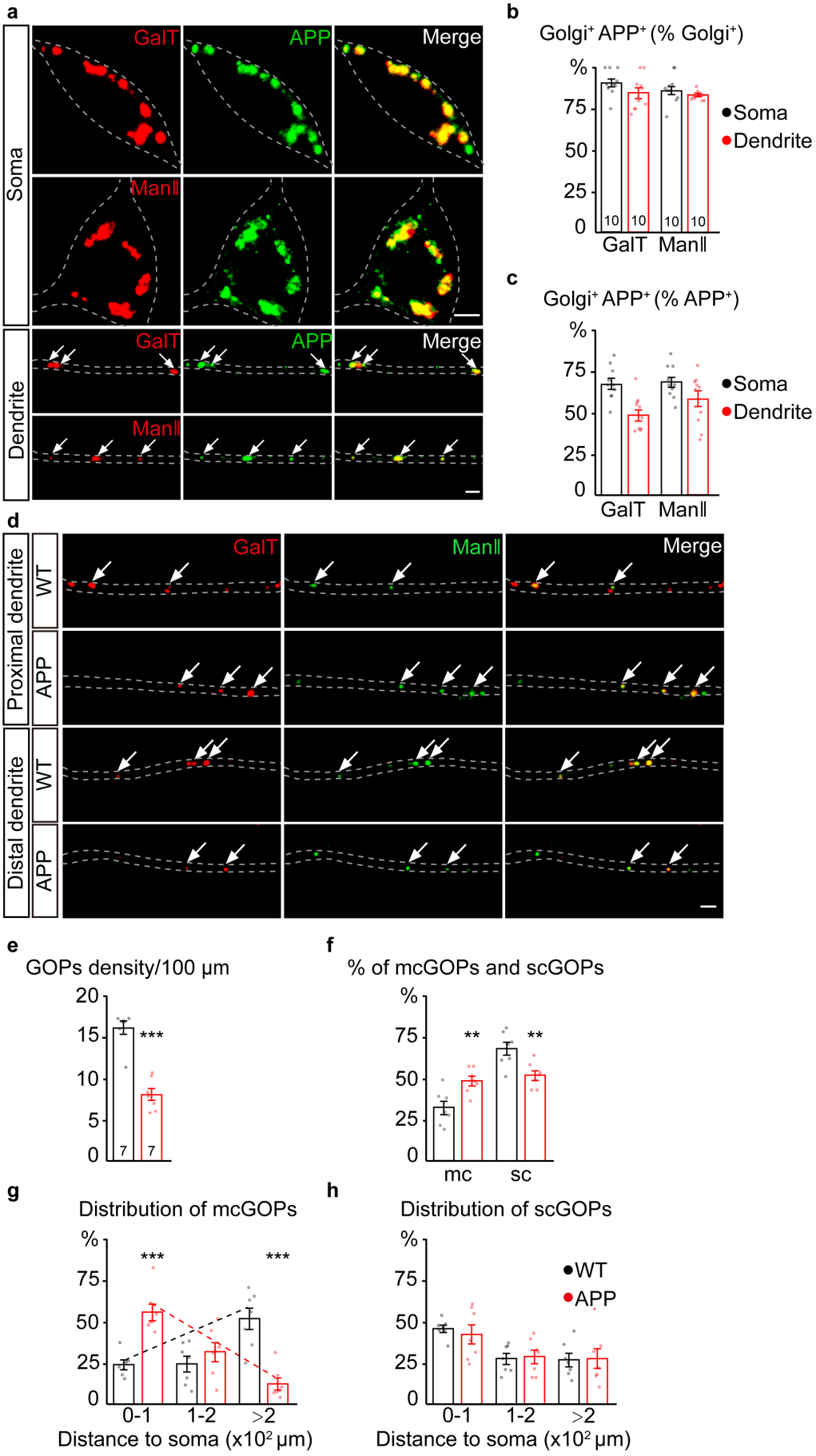
a
Soma
Dendrite
GalT
APP
Merge
ManII
b
Golgi+ APP+ (% Golgi+)
%
75
50
25
0
10
10
10
10
GalT
ManII
Soma
Dendrite
c
Golgi+ APP+ (% APP+)
%
75
50
25
0
GalT
ManII
Soma
Dendrite
d
Proximal dendrite
Distal dendrite
WT
APP
GalT
ManII
Merge
e
GOPs density/100 μm
20
15
10
5
0
***
7
7
f
% of mcGOPs and scGOPs
%
75
50
25
0
**
**
mc
sc
g
Distribution of mcGOPs
%
75
50
25
0
***
***
0-1
1-2
>2
Distance to soma (x10² μm)
h
Distribution of scGOPs
%
75
50
25
0
WT
APP
0-1
1-2
>2
Distance to soma (x10² μm)

542

543 **Fig.2. APP alters the compartmental organization and distribution of GOPs.**

544 **(a)** Examples of APP (green) and Golgi complex (red) in the soma and dendrites. Golgi complex is labeled by GalT
545 (top, *trans*-Golgi) or ManII (bottom, *medial*-Golgi). Arrows indicate colocalized APP and Golgi in dendrites. **(b-c)**
546 Quantification of the proportion of colocalized APP and Golgi complex in soma and dendrites, co-localization as a
547 percentage of Golgi complex (**b**) or APP (**c**). **(d)** Examples of the compartmental organization of dendritic Golgi
548 outposts (GOPs) in wild-type and APP neurons. GOPs are labeled by ManII-GFP (green) and GalT-TagRFPt (red),
549 simultaneously. Arrows point to multi-compartment GOPs (mcGOPs). **(e-h)** Quantification of GOPs in wild-type and
550 APP neurons. **(e)** Density /100 μm, **(f)** the percentage of mcGOPs and scGOPs, **(g-h)** the distribution patterns of **(g)**
551 mcGOPs, and **(h)** scGOPs in dendrites. Scale bar: 2 μm.

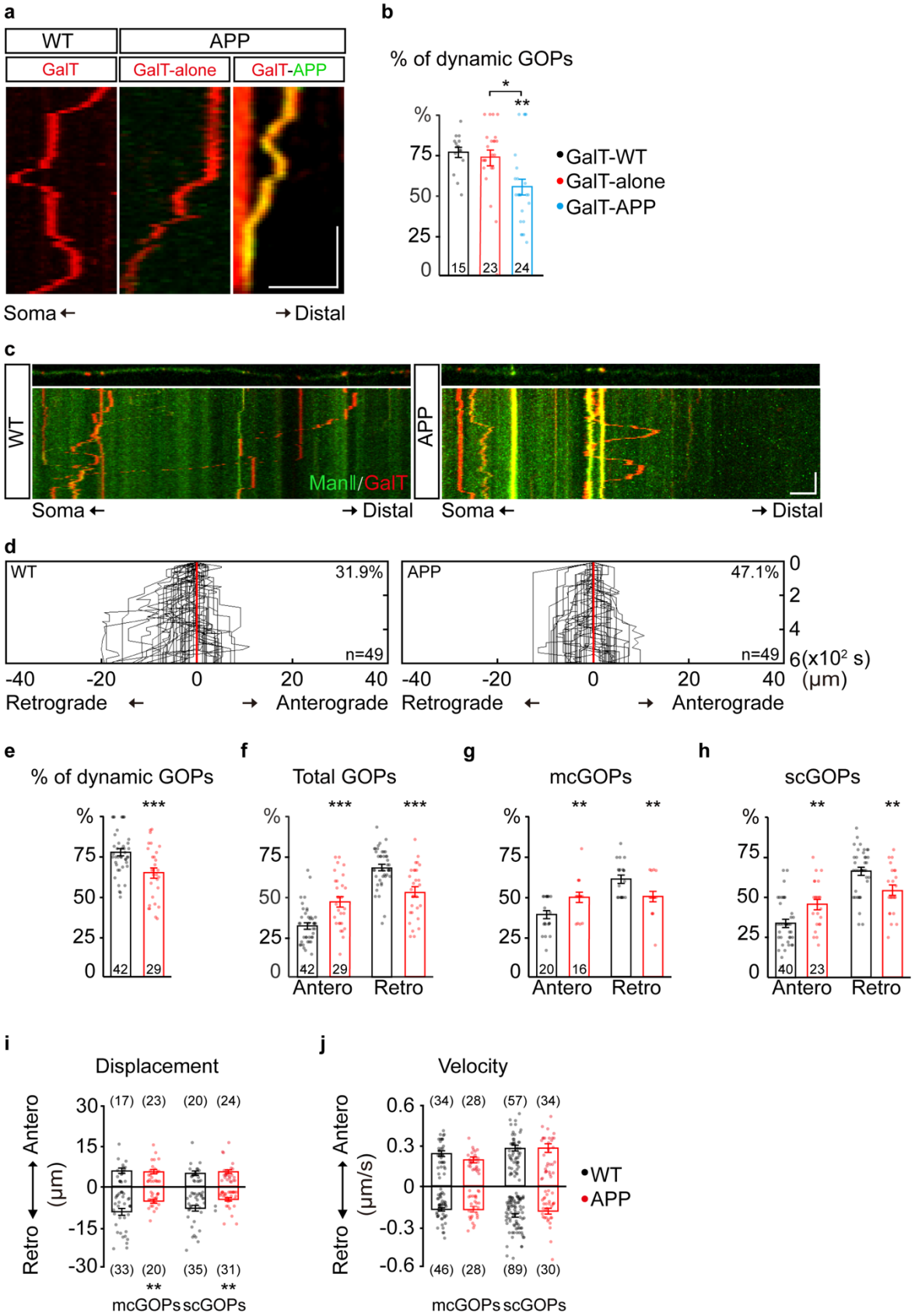
a
WT
APP
GalT
GalT-alone
GalT-APP
Soma ←
→ Distal
b
% of dynamic GOPs
%
75
50
25
0
15
23
24
*
**
GalT-WT
GalT-alone
GalT-APP
c
WT
APP
ManII/GalT
Soma ←
→ Distal
Soma ←
→ Distal
d
WT
31.9%
n=49
APP
47.1%
n=49
-40
-20
0
20
40
Retrograde ←
→ Anterograde
0
2
4
6(x10² s)
(μm)
e
% of dynamic GOPs
***
42
29
f
Total GOPs
***
***
42
29
Antero
Retro
g
mcGOPs
**
**
20
16
Antero
Retro
h
scGOPs
**
**
40
23
Antero
Retro
i
Displacement
Antero
Retro
(μm)
30
15
0
-15
-30
(17) (23) (20) (24)
(33) (20) (35) (31)
**
**
mcGOPs scGOPs
j
Velocity
Antero
Retro
(μm/s)
0.6
0.3
0
-0.3
-0.6
(34) (28) (57) (34)
(46) (28) (89) (30)
WT
APP
mcGOPs scGOPs

553 **Fig. 3. APP disrupts the equilibrium of anterograde/retrograde movements of GOPs.**

554 **(a)** Examples of dynamic GOPs with/without APP**.** Kymograph of time-lapse imaging of GOPs showing GOPs
555 (labeled by GalT-TagRFPt) dynamic without (red) or with APP-GFP (yellow, GalT-APP). **(b)** Bar charts showing the
556 proportion of dynamic GOPs with/without APP. **(c)** Examples of the trajectories of GOPs in wild-type and APP
557 neurons. Top: snapshots of the GOPs in the straightened dendrites. Bottom: kymograph of time-lapse imaging of
558 GOPs. Dual-colors live imaging showing the compartmental organization of GOPs in dendrites, which are labeled
559 by ManII-GFP (green, *medial*-Golgi) and GalT-TagRFPt (red, *trans*-Golgi). Green or red indicates a single-
560 compartment GOP (scGOP) and yellow shows multi-compartment GOP (mcGOP). **(d)** Compound tracks of dynamic
561 GOPs. Red lines are aligned along with displacement 0; puncta numbers and the proportion of anterograde GOPs are
562 indicated within the boxes. (**e-j)** Quantification of GOPs dynamic in wild-type and APP neurons. **(e)** The proportion
563 of dynamic GOPs. **(f-h)** The percentage of anterograde and retrograde movement of GOPs: **(f)** total GOPs, **(g)**
564 mcGOPs, and **(h)** scGOPs. (**i**) Displacement and **(j)** velocity of mcGOPs and scGOPs. Scale bar: 5 μm / 2 min.

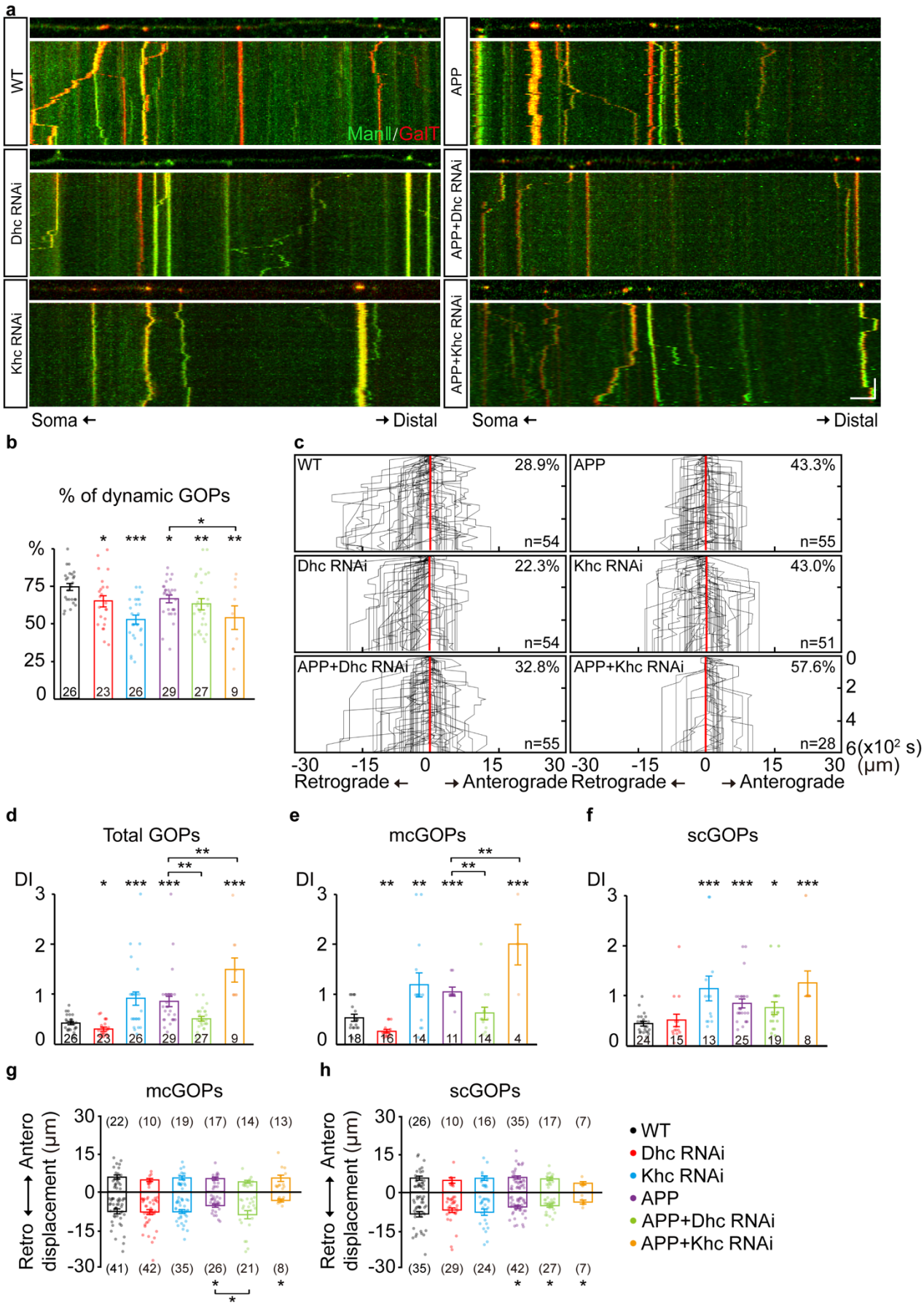
a
WT
Dhc RNAi
Khc RNAi
APP
APP+Dhc RNAi
APP+Khc RNAi
ManII/GalT
Soma ←
→ Distal
b
% of dynamic GOPs
%
75
50
25
0
26
23
26
29
27
9
c
WT
28.9%
n=54
APP
43.3%
n=55
Dhc RNAi
22.3%
n=54
Khc RNAi
43.0%
n=51
APP+Dhc RNAi
32.8%
n=55
APP+Khc RNAi
57.6%
n=28
-30
-15
0
15
30
Retrograde ←
→ Anterograde
6(x10² s)
(μm)
d
Total GOPs
DI
e
mcGOPs
f
scGOPs
g
mcGOPs
Retro ← → Antero
displacement (μm)
h
scGOPs
• WT
• Dhc RNAi
• Khc RNAi
• APP
• APP+Dhc RNAi
• APP+Khc RNAi

566 **Fig. 4. *Dhc* RNAi rescues the alteration of mcGOPs dynamic induced by APP.**

567 **(a)** Examples of the trajectories of GOPs dynamic in wild-type and APP neurons with RNAi knockdown of dynein
568 heavy chain (*Dhc*) or kinesin heavy chain (*Khc*). Top: snapshots of the GOPs in the straightened dendrites. Bottom:
569 kymograph of time-lapse imaging of GOPs in 10 min. Scale bar: 5 μm / 2 min. **(b)** Quantification of the proportion
570 of dynamic GOPs. **(c)** Compound tracks of dynamic GOPs. **(d-f)** Quantification of the direction index (DI) for the
571 GOPs dynamic. The direction index (DI) is calculated using the ratio of anterograde to retrograde movements. **(d)**
572 total GOPs, **(e)** mcGOPs, **(f)** scGOPs. **(g-h)** Quantification of the displacements of (**g**) mcGOPs and (**h**) scGOPs.

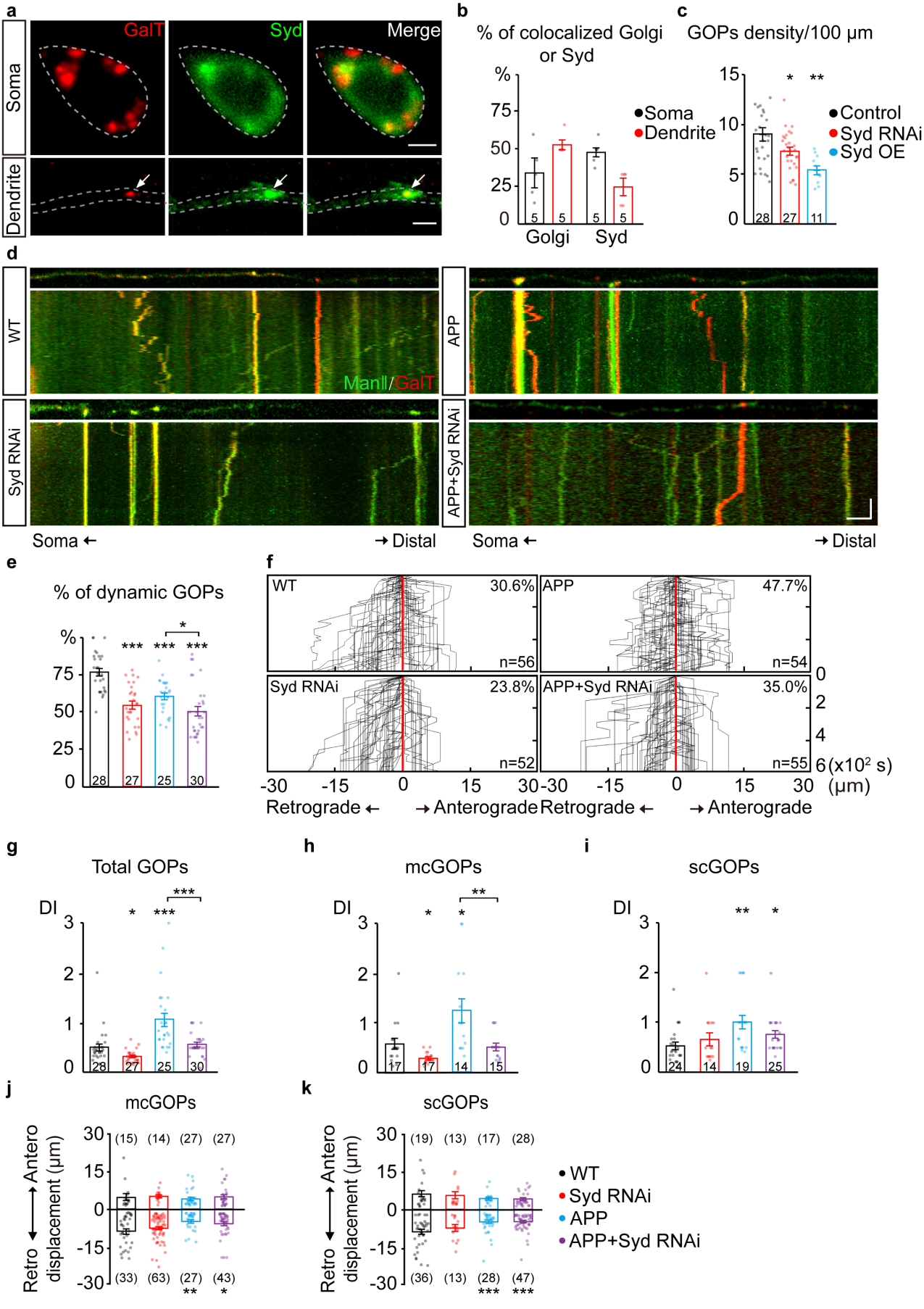
a
Soma
Dendrite
GalT
Syd
Merge
b
% of colocalized Golgi or Syd
Soma
Dendrite
Golgi
Syd
c
GOPs density/100 μm
Control
Syd RNAi
Syd OE
d
WT
APP
Syd RNAi
APP+Syd RNAi
ManII/GalT
Soma ←
→ Distal
e
% of dynamic GOPs
f
WT
APP
Syd RNAi
APP+Syd RNAi
30.6%
47.7%
23.8%
35.0%
n=56
n=54
n=52
n=55
(x10² s)
(μm)
Retrograde ←
→ Anterograde
g
Total GOPs
DI
h
mcGOPs
i
scGOPs
j
mcGOPs
Retro ← → Antero
displacement (μm)
k
scGOPs
WT
Syd RNAi
APP
APP+Syd RNAi

574 **Fig. 5. Syd is required in alteration of mcGOPs dynamic induced by APP.**

575 **(a)** Co-localization of Sunday driver (green, Syd-GFP) with Golgi complex (red, GalT-TagRFPt) in soma and dendrite.
576 Scale bar: 2 μm. **(b)** Quantification of the proportion of colocalized Syd and Golgi complex in soma and dendrites,
577 co-localization as a percentage of Golgi complex (Golgi) or Syd. **(c)** Bar chart showing the density of GOPs following
578 overexpression or knockdown of Syd. **(d)** Examples of the trajectories of GOPs movements in wild-type and APP
579 neurons in Syd knockdown. Top: snapshots of the GOPs in the straightened dendrites. Bottom: kymograph of time-
580 lapse imaging of GOPs in 10 min. Scale bar: 5 μm / 2 min. **(e)** Quantification of the proportion of dynamic GOPs
581 with loss of Syd in wild-type and APP neurons. **(f)** Compound tracks of GOPs dynamic. **(g-j)** Quantification of the
582 direction index (DI) for GOPs dynamic: **(g)** total GOPs, **(h)** mcGOPs, and **(i)** scGOPs. **(j-k)** Quantification of the
583 displacements of (**j**) mcGOPs and (**k**) scGOPs.

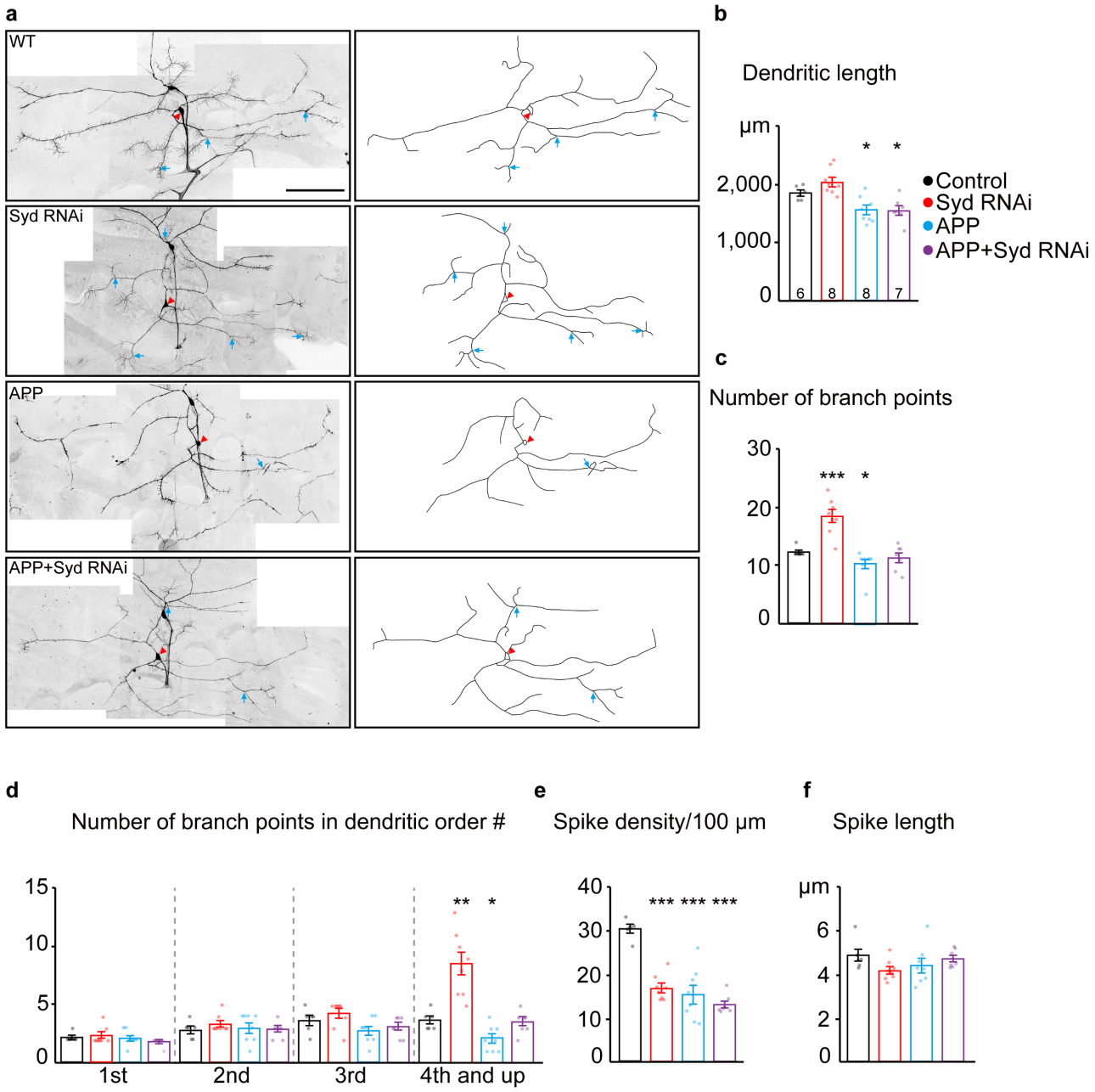
a
WT
Syd RNAi
APP
APP+Syd RNAi
b
Dendritic length
µm
2,000
1,000
0
6
8
8
7
Control
Syd RNAi
APP
APP+Syd RNAi
c
Number of branch points
30
20
10
0
d
Number of branch points in dendritic order #
15
10
5
0
1st
2nd
3rd
4th and up
e
Spike density/100 µm
40
30
20
10
0
f
Spike length
µm
6
4
2
0

585 **Fig. 6. Loss of Syd recovers the dendritic defects induced by APP.**

586 **(a)** The dendritic morphologies of C3da ddaA neurons in wild-type and APP neurons following the loss of Syd. The
587 tracing of the microtubule-based dendritic branches (right). Arrowhead (red) points to the soma and arrows (blue) to
588 the branch points that are at the 4th order and above. Scale bar: 100 μm. **(b-f)** Quantification of the morphological
589 characteristics of C3da neuron. (**b**) Total dendrite length, (**c**) The number of branch points, **(d**) The number of branch
590 points in different orders. (**e-f)** Density (**e**) and length (**f**) of dendritic spikes.